ChemElectroChem

Research Article
doi.org/10.1002/celc.202300295

Chemistry Europe
European Chemical Societies Publishing

www.chemelectrochem.org

Alkylamine-Functionalized Carbon Supports to Enhance the Silver Nanoparticles Electrocatalytic Reduction of CO_2 to CO

Francesco Mattarozzi,[a] Karen van den Akker,[a] Matt L. J. Peerlings,[a] Maaike E. T. Vink-van Ittersum,[a] Nienke L. Visser,[a] Rim C. J. van de Poll,[b] Emiel J. M. Hensen,[b] Peter Ngene,[a] and Petra E. de Jongh*[a]

Silver electrocatalysts enable the conversion of CO_2 to CO, thereby facilitating the transition to a carbon neutral society. To lower the cost of the expensive metal, silver nanostructures are often supported on carbon. This substrate offers great electrical conductivity, but it enhances the selectivity towards the competing hydrogen evolution reaction. In this work, carbon supports were functionalized with linear alkylamines of different chain lengths, to understand its effect on electrochemical performance. Alkylamines interact with the carbon surface and confer hydrophobic properties to the carbon support as well as making the local environment less acidic. These properties led not only to a suppression of the hydrogen evolution, but also to a remarkable enhancement in CO production. Despite the low silver weight loading (0.0016 $mg_{Ag}\,cm^{-2}$), hexylamine-functionalized carbon-based catalysts achieved a CO to H_2 ratio of 2.0, while the same material without the alkylamine functionalization only reached a ratio of 0.3, at −1.3 V vs RHE. This demonstrates the potential of hydrophobic functionalization for enhancing the CO selectivity of carbon-supported catalysts.

Introduction

The electrocatalytic reduction of CO_2 (CO_2RR) combined with direct capture of CO_2 from the air or from concentrated point sources aims to reduce the greenhouse gas net concentrations and to secure carbon neutral fuels.[1] This prospect became even more relevant in recent years,[2] as the price of renewable electricity decreased.[3] However, both the great stability of CO_2 and kinetically slow electron transfer to the reactive species pose challenges to the implementation of this process.[4]

Silver electrodes enable the conversion of CO_2 to CO, thanks to a moderate binding energy of the first reaction intermediate *COOH and a low binding energy of the second intermediate *CO, leading to fast CO desorption.[5,6] Furthermore, supported silver nanostructures offer the opportunity to improve the electrocatalytic performance, while lowering the cost of the expensive metal.[7] Hence, many research groups devoted their efforts to synthesizing size-controlled silver nanoparticles supported on different substrates, such as titania,[8] zeolitic imidazolate frameworks,[9] highly pyrolytic graphite,[10] carbon nitride[11] and glassy carbon.[12]

Carbon-based materials are popular in electrochemistry, due to their low cost, high abundance, great conductivity, and surface tunability.[13] However, they enhance water reduction, producing H_2 as major product and thus lowering the CO_2RR selectivity.[14] To overcome this drawback, strategies to modify the electronic structure of the carbon surface, such as doping the graphitic matrix, were adopted.[15] For instance, imidazole groups were introduced on the surface of oxidized carbon substrates for CO_2RR, resulting in 35% selectivity towards ethanol at −1.0 $mA\,cm^{-2}$.[16]

Functionalization represents an alternative approach to carbon doping. For instance, fluorinated polymers, such as polytetrafluoroethylene (PTFE)[17] and molecules with a long hydrophobic alkyl chain, i.e., 1-octadecathiol,[18] have been used to enhance the hydrophobicity of carbon materials, especially in the context of gas diffusion electrodes. These molecules suppress the H_2 formation by shielding the surface and hampering contact between carbon and water.[19] For instance, the introduction of PTFE onto nickel-embedded nitrogen doped carbon nanotubes significantly improved the catalytic performance of the catalyst, by decreasing the H_2 partial current density by 50%, from −20 $mA\,cm^{-2}$ to −10 $mA\,cm^{-2}$ at −1.2 V, compared to the material without the hydrophobic polymer. This effect was correlated to an increase in contact angle between the electrolyte and the catalyst surface, confirmed by experiments performed with catalysts with different PTFE weight loadings.[20]

Furthermore, Wakerly et al. have shown that 1-octadecanthiol functionalization on the surface of hierarchically structured

[a] F. Mattarozzi, K. van den Akker, M. L. J. Peerlings, M. E. T. Vink-van Ittersum, N. L. Visser, Dr. P. Ngene, Prof. Dr. P. E. de Jongh
Materials Chemistry and Catalysis
Debye Institute for Nanomaterials Science
Utrecht University
Universiteitsweg 99, 3584 CG Utrecht (The Netherlands)
E-mail: p.e.dejongh@uu.nl

[b] R. C. J. van de Poll, Prof. Dr. E. J. M. Hensen
Laboratory of Inorganic Materials and Catalysis
Department of Chemical Engineering and Chemistry
Eindhoven University of Technology
P. O. Box 513, 5600 MB Eindhoven (The Netherlands)

Supporting information for this article is available on the WWW under https://doi.org/10.1002/celc.202300295

copper dendrites not only suppressed the H_2 evolution, from 60% faradaic efficiency (FE)

0to 10% FE (hydrophobic electrode) at −1.6 V, but also boosted the activity towards CO_2RR, increasing the C_1 products selectivity from 10% to 30% at the same potential.[21] This observation was attributed to the ability of the hydrophobic copper electrodes to trap CO_2 bubbles at the electrode surface, resulting in a higher local concentration of CO_2 near the electrode surface.[22]

In this work, for the first time we functionalized hydrophilic graphitic carbon materials with different alkylamines *via* a one-step procedure, systematically varying the alkyl chain length ($6 \leq$ alkyl carbon atoms ≤ 18). Furthermore, we investigate how alkylamine functionalization on carbon affects both the physical-chemical properties of the carbon and its electrocatalytic performance in CO_2RR. A low weight loading of colloidal silver nanoparticles (0.0016 $mg_{Ag}\,cm^{-2}$) was drop casted onto the functionalized electrodes to enable the CO_2 conversion to CO. We show that this approach leads to an increase in CO production and suppression of water reduction. At −1.4 V vs. RHE, the hexylamine-functionalized carbon catalyst enabled both a 40% reduction in H_2 partial current density and a 225% increase in CO partial current density compared to the hydrophilic benchmark material. These results open the possibility to apply the same method for the preparation of gas diffusion electrodes.

Results and Discussion

Synthesis of silver nanoparticles

Figure 1a shows the transmission electron microscopy (TEM) image of the as-synthesized colloidal silver nanoparticles and particle size distribution (inset). The silver nanoparticles had an average particle size of 8.2 nm, and a narrow particle size distribution (standard deviation = 0.7 nm, Figure 1a inset). The TEM image (Figure 1a) demonstrates that most nanoparticles had a spherical morphology. Additional structural characterization using UV-vis measurements (Figure S1) confirmed the formation of small and mono-dispersed silver nanoparticles.[23] To investigate the surface and bulk oxidation state of the silver nanoparticles, both X-ray photoelectron spectroscopy (XPS) and X-ray diffraction (XRD) analysis were performed. Figure 1b shows that the surface of the silver nanoparticles is in the Ag^0 state, as evidenced by the presence of metallic silver peaks, with the 3d features at 368.4 eV and 374.5 eV. The XRD pattern (Figure 1c) clearly shows the (111), (200), (220) and (311) Bragg reflections of silver, confirming successful synthesis of face centered cubic metallic bulk silver nanoparticles. By applying the Scherrer equation to the peak broadening in the XRD pattern, an average crystallite size of 4 nm was calculated. This is smaller than the particle size (8.2 nm) measured by TEM, suggesting either polycrystalline particles or the presence of amorphous silver.

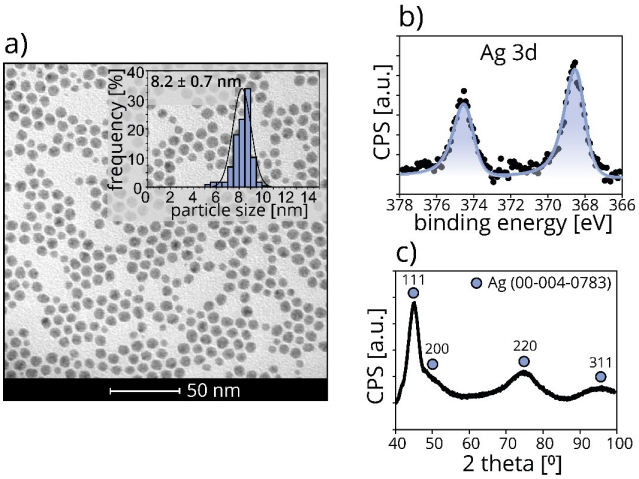

Figure 1. a) TEM image of colloidal silver nanoparticles and particle size distribution (inset). b) XPS spectrum of silver nanoparticles supported on a carbon paper electrode. c) XRD pattern of colloidal silver particles drop casted on top of a (911) single crystal silicon wafer.

Carbon functionalization

Table 1 summarizes the carbon (C), oxygen (O) and nitrogen (N) atomic percentages of the functionalized carbon powders before loading with silver nanoparticles. These data were obtained from the XPS survey spectra (Figure S2). GNP-O_0 C, the benchmark carbon material obtained by liquid phase oxidation of commercial graphitic carbon, displayed the highest content of oxygen (8.4 at%), and the lowest percentage of carbon and nitrogen, corresponding to 91.0 at% and 0.5 at%, respectively. The carbon content in GNP-HA_6 C and GNP-OA_8 C was 93.0 at%, with a similar oxygen content of 5.5 at% and 5.3 at%, respectively and similar nitrogen content of 1.5 at% and 1.7 at%. GNP-ODA_18 C displayed the highest carbon content (96.0 at%) and nitrogen content (2.1 at%), and the lowest oxygen content (1.9 at%). The increase in carbon content and decrease in oxygen content from GNP-O_0 C to GNP-ODA_18 C is explained by the increasingly longer carbon chains, from 0 to 18 carbon atoms, shielding the oxygen atoms of the carbon support surface. This hypothesis is supported by the higher surface sp^3 character of the alkyl amine functionalized carbon materials (Figure S3, Table S1), which is different from the high sp^2 percentage in GNP-O_0 C, calculated as the D-parameter from the carbon Auger peak. No significant differences in crystallinity for the different carbon materials

Table 1. XPS carbon (C), oxygen (O) and nitrogen (N) atomic percentages of GNP-O_0 C, GNP-HA_6 C, GNP-OA_8 C and GNP-ODA_18 C functionalized carbon powders without silver nanoparticles.

Sample ID	C atomic%	O atomic%	N atomic%
GNP-O_0 C	91.0	8.4	0.5
GNP-HA_6 C	93.0	5.5	1.5
GNP-OA_8 C	93.0	5.3	1.7
GNP-ODA_18 C	96.0	1.9	2.1

were observed from the XRD results, comparing directly before (Figure S4a) and after (Figure S4b) catalysis. The increase in nitrogen content for GNP-HA_6 C, GNP-OA_8 C and GNP-ODA_18 C is attributed to the amine functionality of the alkylamines.

To further investigate the chemical nature of the nitrogen atoms, the high-resolution N 1s XPS spectra were deconvoluted and the abundance of the different N species was quantified (Figure 2). GNP-O_0 C (Figure 2a) showed only native pyrrolic groups, while the alkylamine functionalized carbons showed different ratios between amine (R–NH_2, pink) at 400 eV and protonated amine (R–NH_3^+, blue) groups at 402 eV (Figure 2b–d).[24] These results demonstrate that a fraction of the alkylamines was simply physically adsorbed at the surface of the carbon powder (R–NH_2 peak), while part of the alkylamines electrostatically interacted with the acidic carbon surface groups (R–NH_3^+ peak).[25]

Figure 2e shows the atomic ratio of the protonated to adsorbed amine groups as a function of the number of carbon atoms in the linear alkyl chains. GNP-HA_6 C showed the highest ratio (0.55), followed by GNP-OA_8 C (0.44) and GNP-ODA_18 C (0.23). This means that the longer alkyl chains interact less strongly with the polar surface groups. This could be due to steric hindrance of the alkyl chain, which limits the electrostatic interaction with the acidic surface groups of the carbon. After spraying the functionalized carbon onto the carbon paper, the ratio between protonated amines and free amines increased (Figure S5), suggesting a weak interaction between the physically adsorbed amines (R–NH_2 peak at 400 eV) and the surface of the oxidized carbon.

These results indicate that the GNP-O carbon was successfully functionalized with the alkylamines, as further evidenced by the point of zero charge analysis, measured via mass titration (Table S2). This analysis showed that starting from the acidic GNP-O_0 C surface (point of zero charge (PZC) = 3.1), modification with the alkylamines neutralized the acidic sites, leading to a nearly neutral surface (PZC ~ 7).

Carbon supported silver nanoparticles (electrodes)

To prepare the electrode materials, the oxidized (GNP-O_0 C) and hydrophobic functionalized (GPN-HA_6 C, GNP-OA_8 C and GNP-ODA_18 C) carbon materials were sprayed onto a carbon paper support. After this, a low loading (0.0016 $mg_{Ag}\,cm^{-2}$) of colloidal silver nanoparticles was drop cast onto the electrodes. As the main aim of the alkylamine functionalization was to decrease the wettability of the carbon surface, the hydrophilic/hydrophobic properties of the carbon supported silver nanoparticle electrodes were determined using contact angle measurements.

Figure 3 shows representative contact angle images for a) GNP-O_0 C, b) GNP-HA_6 C, c) GNP-OA_8 C and d) GNP-ODA_18 C catalysts with 0.0016 $mg_{Ag}\,cm^{-2}$, while Figure 3e gives the contact angles as a function of the alkylamine chain length. GNP-O_0 C possessed a moderately hydrophilic character, with a 71° contact angle. GNP-HA_6 C and GNP-OA_8 C were most hydrophobic, with contact angles of 109° and 110°, respectively. GNP-ODA_18 C exhibited a 100° contact angle, slightly lower than GNP-HA_6 C and GNP-OA_8 C. The hydrophilicity of GNP-O_0 C is explained by the presence of O-containing polar groups, which enhanced the wettability of the electrode. The hydrophobicity of GNP-HA_6 C and GNP-OA_8 C was due to the poor interaction between the long alkyl chains of the alkylamine moieties and water. This shows that the hydrophilic

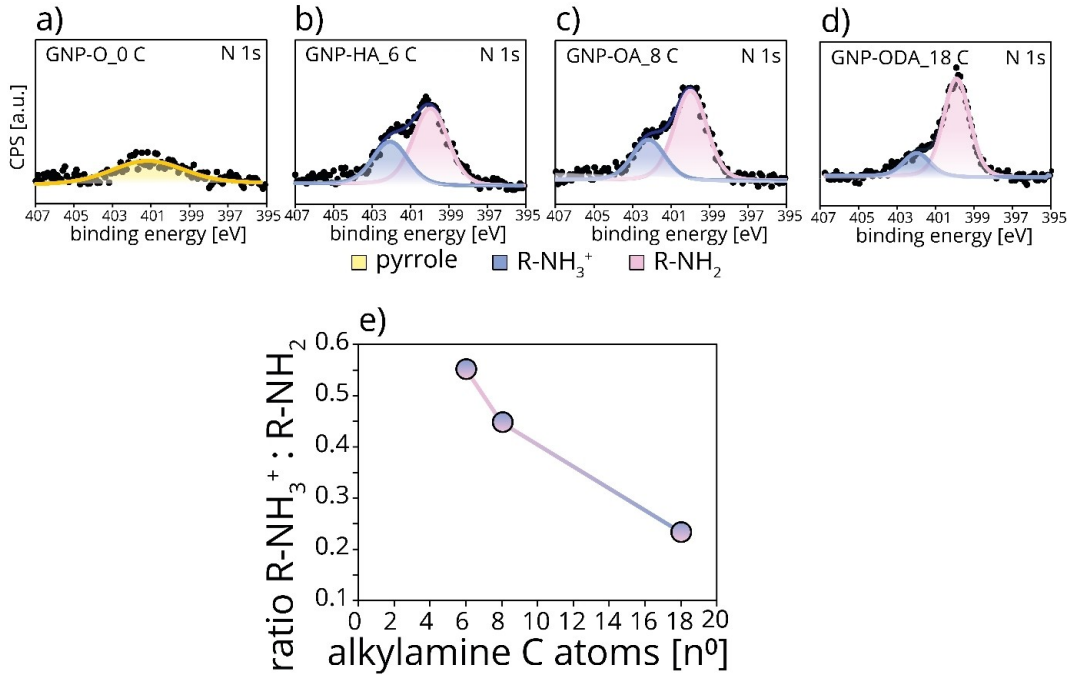

Figure 2. XPS spectrum of a) GNP-O_0 C, b) GNP-HA_6 C, c) GNP-OA_8 C and d) GNP-ODA_18 C functionalized carbon powders without silver nanoparticles. e) Ratio between protonated amine (R–NH_3^+) and free amine (R–NH_2) as a function of the alkyl amine chain length for the functionalized samples.

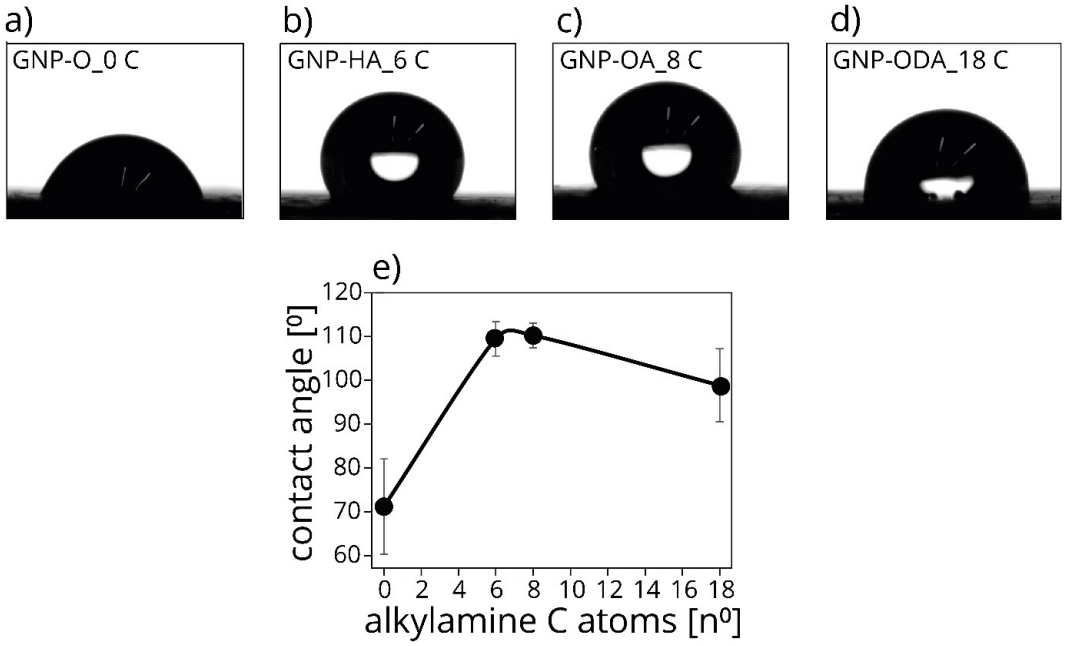

Figure 3. Photos of 4 µL of water on the surface of a) GNP-O_0 C, b) GNP-HA_6 C, c) GNP-OA_8 C and d) GNP-ODA_18 C functionalized carbon electrodes with silver nanoparticles. e) Contact angles as a function of the alkyl amine chain length.

O-containing groups were successfully shielded by the alkylamine hydrophobic chains. GNP-ODA_18 C showed a slightly less hydrophobic surface compared to GNP-HA_6 C and GNP-OA_8 C. This indicates that the different hydrophobicity cannot be explained solely by the length of the alkylamines, but possibly other factors, such as a different surface morphology, and/or a different dispersion of functionalized carbon on the electrode surface for long alkyl chains.

To further investigate the origin of the difference in hydrophobicity, scanning electron microscopy (SEM) measurements were performed. Figure 4 shows low magnification (top) and high magnification (bottom) SEM images of GNP-O_0 C, GNP-HA_6 C, GNP-OA_8 C and GNP-ODA_18 C electrodes. GNP-O_0 C, GNP-HA_6 C and GNP-OA_8 C possessed a qualitatively similar distribution of carbon particles over the fibers of the carbon paper. All three catalysts were uniformly coated on the carbon fibers (low magnification images) with sharp-edged

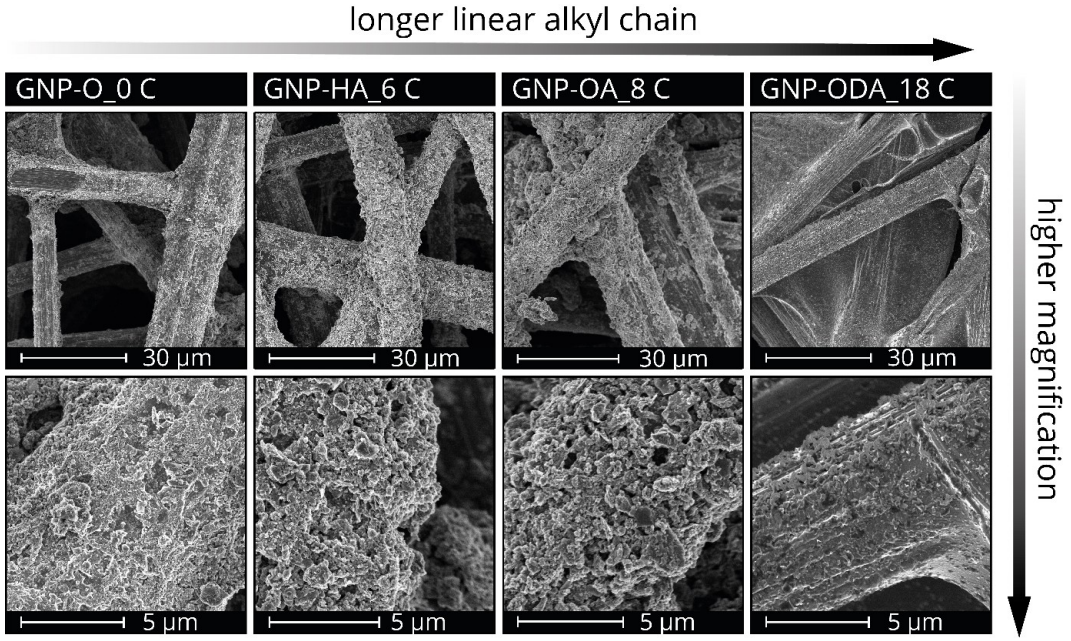

Figure 4. Scanning electron microscopy (SEM) images of GNP-O_0 C, GNP-HA_6 C, GNP-OA_8 C and GNP-ODA_18 C carbon electrodes with Ag nanoparticles.

particles (high magnification images). GNP-ODA_18 C showed a non-uniform distribution of the carbon powder, with most of carbon fibers of the substrate not covered by the soft-edged particles. As the carbon paper is less hydrophobic than the functionalized carbon material, the water-carbon contact angle is expected to be lower. Hence, the different carbon paper coverages between the catalysts might contribute the lower hydrophobicity for GNP-ODA_18 C, compared to the other alkyl functionalized catalysts.

Furthermore, the catalysts morphology did not significantly change during catalysis, as clear form a comparison of the SEM results before (Figure 4) and after-catalysis SEM images (Figure S6).

Electrocatalytic performance: influence of hydrophobic functionalization on the catalysts' selectivity

To investigate the effect of hydrophobic functionalization on the total current density (Figure 5) and selectivity (Figure 6), potentiostatic measurements were performed in 0.1 M $KHCO_3$, applying each potential for 30 minutes. Both figures have been simplified, but the full range of potentials measured is reported in Figure S7 and Figure S8. Figure 5 shows the geometric total current density for the four catalysts, as a function of the applied potential. The electrocatalysts generated similar current densities at low overpotentials, up to −1.1 V. At more negative potentials, GNP-ODA_18 C showed the smallest current densities, with only −1.6 mA cm^{-2} and −2.8 mA cm^{-2} at −1.2 V and −1.4 V respectively. In the same potential range, GNP-O_0 C, GNP-HA_6 C and GNP-OA_8 C produced similar current densities. These catalysts produced their largest current density at −1.4 V, with −3.7 mA cm^{-2} for both GNP-O_0 C and GNP-OA_18 C, and −4.3 mA cm^{-2} for GNP-HA_6 C. The small current density generated by GNP-ODA_18 C could be explained by non-uniform distribution of the functionalized carbon catalysts, which left a large fraction of the low activity carbon fibers of the carbon paper bare.

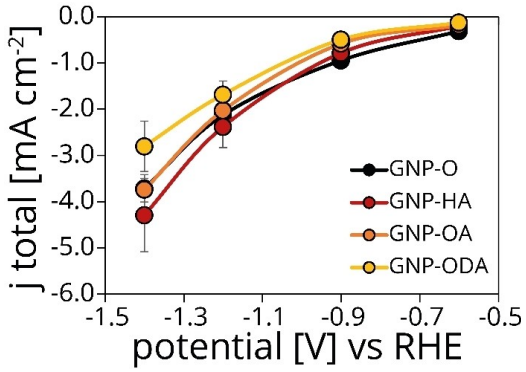

Figure 5. Geometric total current densities as a function of the applied potential. Each data point corresponds to the average current measured by chronoamperometry applying a constant potential for 30 minutes.

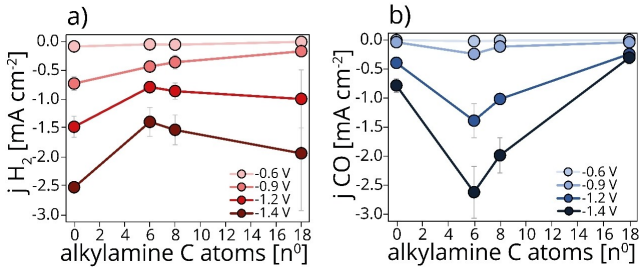

Figure 6. a) H_2 and b) CO partial current density as a function of the number of carbon atoms in the alkyl chain, measured by chronoamperometry applying a constant potential for 30 minutes.

To separate the contribution of water reduction and the CO_2RR to the total current and thereby probe the influence of the hydrophobic functionalization on the selectivity, the H_2 and CO partial current densities were calculated based on the CO and H_2 product formation rates as a function of the alkyl chain length. This analysis was derived by combining the faradaic efficiency data (Figure S9) and the total current densities. Figure 6a clearly shows that the alkylamine functionalization suppressed the H_2 partial current density. GNP-O_0 C was undoubtfully the catalyst with the highest H_2 production, both at low and high overpotentials, generating a maximum of −2.5 mA cm^{-2} at −1.4 V. GNP-HA_6 C and GNP-OA_8 C showed the lowest overall hydrogen production, with only −1.4 mA cm^{-2} and −1.5 mA cm^{-2} respectively at the largest overpotential. The suppression of the hydrogen evolution reaction for the alkylamine functionalized catalysts is mainly ascribed to a lower wettability of the hydrophobically functionalized materials (Figure 3), leading to limited water accessibility to the carbon surface. The difference in local environment between GNP-O_0 C and the other catalysts might also play a role in the suppression of the H_2 evolution reaction, as the alkylamine functionalization shields the acidic surface groups on the carbon surface, leading to a less acidic pH close to the electrode surface. This might be relevant especially in the low potential range, where the total current density is small, and the proton consumption is limited.

Also, the CO partial current density (Figure 6b) was greatly influenced by the functionalization. GNP-HA_6 C and GNP-OA_8 C produced a larger current density than the activated carbon GNP-O_0 C and GNP-ODA_18 C. At −1.2 V, both GNP-HA_6 C and GNP-OA_8 C generated a 3.5- and 6.6- fold CO partial current density enhancement compared to GNP-O_0 C and GNP-ODA_18 C, respectively. Under the largest potential bias (−1.4 V), GNP-HA_6 C produced −2.6 mA cm^{-2}, while GNP-O_0 C, GNP-OA_8 C and GNP-ODA_18 C displayed only −0.8 mA cm^{-2}, −2.0 mA cm^{-2} and −0.3 mA cm^{-2}, respectively. The same trend was found by calculating the CO partial current density normalized by silver surface area, as a function of the applied potential (Figure S10).

The remarkable enhancement in CO production observed for GNP-HA_6 C and GNP-OA_8 C could be explained by a thin gas layer trapped near the surface of the functionalized electrodes, which increases the local concentration of CO_2 at the electrode surface.[21] GNP-ODA_18 C performed worse than GNP-O_0 C. The 18-carbon atom chain might shield the active sites for CO_2RR (silver nanoparticles). Control experiments on the modified carbon electrodes without silver nanoparticles

confirmed that the alkylamine functionalization alone did not steer the selectivity towards CO (Figure S11).

An important parameter is the produced ratio of CO to H_2 (Figure 7). At low overpotentials, all the alkyl functionalized materials outperformed GNP-O_0 C. At −1.2 V, GNP-ODA_18 C generated a CO to H_2 ratio of 0.3, like GNP-O_0 C, while GNP-OA_8 C and GNP-HA_6 C showed a ratio of 1.2 and 1.7, respectively. At −1.3 V, GNP-HA_6 C reached the maximum CO to H_2 ratio, equal to 2.0, while GNP-OA_8C, GNP-O_0 C and GNP-ODA_18 C only produced a ratio of 1.3, 0.3 and 0.2. At more cathodic biases, the catalysts seem to reach a plateau, indicating no further improvement in CO selectivity.

In literature, higher electrocatalytic performance is obtained using highly optimized systems, such as a remarkable $FE_{CO} >$ 90% reported by J. Chen et al.[26] However, in the present study we show a new strategy to reduce the competitive hydrogen evolution reaction and steer the selectivity towards CO production for carbon-based electrodes. This was successfully achieved by introducing hydrophobic functional groups on the surface of activated carbons.

Conclusions

A series of four modified carbon materials, functionalized either with oxygen-containing groups (GNP-O_0 C, benchmark) or with amines with different number of carbon atoms in the linear alkyl chain, i.e., hexylamine (GNP-HA_6 C), octylamine (GNP–OA_8 C) and octadecylamine (GNP-ODA_18 C) was produced. 0.0016 $mg_{Ag}\,cm^{-2}$ of colloidal silver nanoparticles (8.2 nm diameter) was drop cast on the carbon materials. Both XPS and contact angle measurements demonstrated that the alkylamines were successfully deposited on the carbon, making the electrode surface more hydrophobic and less acidic. The alkylamine functionalized carbons exhibited significantly lower H_2 partial current densities and increased CO current densities compared to the oxygen functionalized carbon. This clearly shows that alkylamine functionalization is beneficial for the electrocatalytic performance of carbon-based electrodes for CO production.

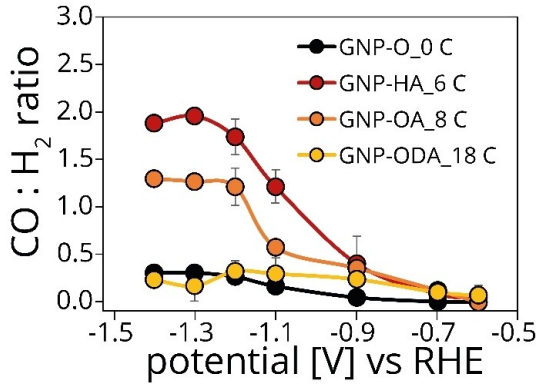

Figure 7. CO to H_2 ratio as a function of the applied potential.

Experimental section

Synthesis of silver nanoparticles

Silver nanoparticles were prepared via colloidal synthesis, by reducing silver nitrate with trioctylamine, and using tetradecyl phosphonic acid and oleic acid as capping agents.[27] In summary, 170 mg of $AgNO_3$ (99.5%, Sigma Aldrich) and 278 mg of tetradecyl phosphonic acid (capping agent, 98.0%, Sigma Aldrich) were placed in a 100 mL three neck flask equipped with a condenser and a Teflon stirring bar. 20 mL of 1-octadecene (synthesis grade, Sigma Aldrich) was added as solvent. 0.7 mL of oleic acid (capping agent, 99.0%, Sigma Aldrich) and 1.0 mL trioctylamine (reducing agent, 98.0%, Sigma Aldrich) were added to the mixture. The flask was evacuated for 1 hour at room temperature. Subsequently, N_2 was introduced, and the temperature was quickly increased to 60 °C. The thermocouple connected to the heating mantle, was immersed in the solution inside a glass shell (Figure S12) to avoid metal contamination. After 30 minutes at 60 °C, the solution turned from pale yellow to dark brown, indicating the formation of silver nanoparticles. Then, the solution was heated up to 100 °C and the temperature was held for 30 minutes. The solution was cooled down to room temperature. The final product was washed three times in 1 mL hexane (95.0%, Sigma-Aldrich) and 20 mL ethanol (99.5%, VWR chemicals). Between each washing step, the solution was centrifugated at 3000 rpm for 10 minutes, the solvent was decanted, and the product was collected at the bottom of the centrifuge tube. Finally, the solution was resuspended in hexane and stored in a glass vial, protected from direct light by an aluminum foil wrapped around it.

Synthesis of functionalized carbon powders

The synthesis of the oxidized carbon substrate (GNP-O_0 C) has been described in a previous publication.[28] In summary, 10 g of commercial graphitic nanoplatelets powder (GNP-500, grade C, XG-Science) was dispersed in HNO_3 (65.0% wt/wt, Sigma Aldrich), heated to 80 °C for 2 hours. The product was washed four times with deionized water, dried for 12 hours at 90 °C and ground in a mortar. Oxidized carbon materials were used as substrate for the alkylamine functionalization as they have enhanced interaction with the functionalizing molecules due to the carboxylic groups present on their surface.

The alkylamine functionalized carbons were produced by direct thermal mixing.[29–31] 0.2 g of GNP-O_0 C was dispersed in 40 mL milli-Q water in a 100 mL three neck round bottom flask equipped with a condenser and a Teflon stirring bar. 1.1×10^{-3} moles of alkylamine were added. After 15 minutes of sonication, the solution was heated to 100 °C for 20 hours at 400 rpm stirring rate. After cooling down to room temperature, the suspension was filtered, washed with milli-Q water, dried at 90 °C, and ground in a mortar. GNP-HA_6 C denotes the carbon functionalized with hexylamine (HA, 99.0%, Sigma Aldrich), GNP-OA_8 C functionalized with octylamine (OA, 99.5%, Acros Organics) and GNP-ODA_18 C the carbon functionalized with octadecylamine (ODA, 99.0%, Sigma Aldrich). The numbers following GNP-O, GNP-HA, GNP-OA and GNP-ODA indicates the number of carbon atoms in the linear alkyl chain of the alkylamines.

Synthesis of functionalized carbon electrodes

The cathodes were prepared by spraying the functionalized carbons onto a 4.9 cm^2 carbon paper substrate (Toray TGP-H-060). 11 mg of functionalized carbon was dispersed in 4470 µL milli-Q water, 1120 µL isopropanol (99.0%, Sigma Aldrich) and 44 µL Nafion

solution (5.0% in water and 1-propanol, Alfa Aesar) and sonicated for 45 minutes. After sonication, a weight loading of 0.3 $mg_{carbon}\,cm^{-2}$ was applied by spraying the ink over the carbon paper, using a Conrad HP-200 Airbrush-Pistole. The modified carbon electrodes were dried overnight under vacuum at room temperature. Finally, a silver loading of 0.0016 $mg_{Ag}\,cm^{-2}$ on the carbon electrode was deposited by drop casting the colloidal silver nanoparticles onto the electrode.

Characterization

Images of colloidal silver particles were acquired by transmission electron microscopy (TEM) using a Thermo Fischer Scientific Tecnai 20 microscope, operated at 200 kV. The TEM grids were prepared by drop casting the silver nanoparticles colloidal solution onto a holey carbon 200 mesh copper grid. The silver nanoparticle average diameter was calculated by taking into account 5 different TEM images and 145 particles in total. The average diameter was calculated as Equation (1):

$$d_{avrg} = \frac{\sum_i^n d_n}{N} \quad (1)$$

where d_n is the diameter of particle n, and N is the total number of particles counted. UV-vis spectra were recorded using Agilent Technologies Cary 60 UV-Vis. X-ray diffraction measurements both for the silver nanoparticles and functionalized carbon electrodes were performed on a Bruker D2 Phaser, equipped with a Co K_α X-ray source with a wavelength of 1.79026 Å. The colloidal silver nanoparticles were drop cast onto a (911) single crystal silicon wafer before the XRD measurement, to maximize the signal to noise ratio.

Scanning electron microscopy (SEM) images were acquired on a Helios G3UC operated at 2 kV and the contrast in the final images was adjusted using ImageJ software. The XPS data were collected using a ThermoFischer Thermo Scientific K-Alpha X-ray Photoelectron Spectrometer, with an Al source (Kα monochromatic radiation 1486.6 eV). The deconvolution and quantification of the silver peaks was achieved using CasaXPS. The energy scale was calibrated by setting the C 1s of adventitious carbon to a binding of 284.8 eV. For GNP-ODA_18 C, this approach was not possible, due to the insulating properties of the long alkyl amine, leading to a significant shift of the carbon peak due to the surface charging.[32,33] In this case, the O 1s peak was set to 532.7 eV, the O feature belonging to the activated carbon GNP-O_0 C. All the N peaks, deconvoluted using an LA Lorentzian asymmetric (1.53; 243) line shape, have the same full width at half maximum (FWHM) within each sample. A small degree of variation is detected for FWHMs of different samples, ranging from 1.7 to 2.1. The only exception is the large broad pyrrolic peak present in GNP-O_0 C with a 4.5 FWHM, which only testifies that the low concentration of native N-groups on the pristine carbon material make it difficult to deconvolute XPS peaks. The D-parameter and relative sp^2–sp^3 character of the functionalized carbon materials were calculated as the distance in between the minimum and maximum of the first differential of the carbon Auger peak. A linear relationship between the calculated D-parameter and the sp^2–sp^3 character of the carbon was assumed. The extremes of the series are diamond, which is fully sp^3 with a D-parameter of 14, and higly oriented graphite, which is fully sp^2 with a D-parameter of 24.[34]

To determine the silver metal weight loading on the carbon paper support, the concentration of colloidal silver nanoparticles was measured by atomic absorption spectroscopy on a ContrAA 700 AAS instrument and multiplied by the amount of solution drop casted onto the electrodes. The contact angle measurements were performed on a Dataphysics OCA 15plus instrument, with water droplets of 4 μL.

Electrocatalytic measurements

A polymethylmethacrylate (PMMA) three-electrode H-type cell was used for all the electrocatalytic experiments (Figure S13). 15 mL electrolyte solution (0.1 M $KHCO_3$, pH = 6.8, 99.0%, Sigma Aldrich) was added to both the cathodic and anodic compartments (headspace volume = 3 mL each). The two compartments were divided by a Nafion 117 membrane (Ion Power). A flowrate of 10 mL min^{-1} CO_2 (Linde, purity 5.2) was applied for 1 hour prior to the experiments, to saturate the catholyte. The same CO_2 flowrate was applied during the experiments. Ar (10 mL min^{-1}) was bubbled through the anolyte solution. The working electrode was made of a glassy carbon disc (HTW-Germany) and the carbon paper disc (4.9 cm^2, TGP-H-060, Toray), directly in contact with the electrolyte. The functionalized carbon catalysts (0.3 $mg_{carbon}\,cm^{-2}{}_{carbon\ paper}$) and the colloidal silver nanoparticles (0.0016 $mg_{Ag}\,cm^{-2}{}_{carbon\ paper}$) were deposited onto the carbon paper. The carbon paper surface area in contact with the electrolyte was 3.8 cm^2. A Ag/AgCl (3 M KCl) reference electrode (Metrohm) was used, while a 3.8 cm^2 Pt disc (99.5%; Goodfellow) was used as counter electrode. The electrochemical measurements were performed using a Autolab PGSTAT204 potentiostat, and the applied potential was converted to the reversible hydrogen electrode potential (RHE) using the equation: $E_{RHE} = E_{Ag/AgCl} + 0.199 + 0.059\ pH$. The electrocatalytic performance was measured by chronoamperometry experiments, in which seven potentials per experiment were tested. Each potential was applied for 30 minutes.

The gaseous products were analyzed by gas chromatography, using Global Analysis Solution Microcompact GC 4.0 machine from InterScience, described in detail in a previous paper.[28] Only CO and H_2 were detected as gaseous products and therefore included in the selectivity calculation. The selectivity of the process was defined by the FE, calculated as Equation (2):

$$FE = \frac{(n^* F\ ^*\mathrm{mol})}{i_{tot}{}^* t} \quad (2)$$

where n is the moles of electrons per mole of product [$mol_{e^-}\ mol_P^{-1}$], F is the Faraday constant [$C\,mol_{e^-}{}^{-1}$], mol is the moles of products formed [mol_P], i is the total current [$C\,s^{-1}$] and t is the analysis time [s]. The partial current density defines the individual contribution of the reaction products to the total current density. This parameter was calculated as the product of the total current density and the FE.

All electrocatalytic data shown in this manuscript were the average of three experiments performed on two different batches of functionalized carbons and silver nanoparticles, synthesized, and tested by two different operators. The error bars were calculated using the standard deviation.

Acknowledgements

Francesco Mattarozzi and Rim van de Poll were funded by the Dutch Research Council (NWO), via the Advanced Research Center Chemical Building Blocks Consortium (ARC-CBBC) in collaboration with Shell Global Solutions International B.V. Matt Peerlings and Maaike Vink-van Ittersum acknowledge funding

from the NWO and RELEASE consortium. Nienke Visser was funded by TotalEnergies OneTech Belgium. Stephan Jonker is acknowledged for the precious help with atomic absorption spectroscopy measurements. Alex van Silfhout is acknowledged for his help during the contact angle measurements. Jan Willem de Rijk is acknowledged for the technical support, helping both with the cell design and the preparation of the catalytic set-up during this project. Valerio Gulino is acknowledged for the useful discussions related to the project results.

Conflict of Interests

The authors declare no conflict of interest.

Data Availability Statement

The data that support the findings of this study are available from the corresponding author upon reasonable request.

Keywords: silver nanoparticles · carbon · CO_2 reduction · hydrophobicity · alkylamine.

[1] D. L. T. Nguyen, Y. Kim, Y. J. Hwang, D. H. Won, *Carbon Energy* **2020**, *2*, 72–98.
[2] R. Kas, K. Yang, D. Bohra, R. Kortlever, T. Burdyny, W. A. Smith, *Chem. Sci.* **2020**, *11*, 1738–1749.
[3] D. Bogdanov, M. Ram, A. Aghahosseini, A. Gulagi, A. S. Oyewo, M. Child, U. Caldera, K. Sadovskaia, J. Farfan, L. De Souza Noel Simas Barbosa, M. Fasihi, S. Khalili, T. Traber, C. Breyer, *Energy* **2021**, *227*, 120467.
[4] Z. Sun, T. Ma, H. Tao, Q. Fan, B. Han, *Chem* **2017**, *3*, 560–587.
[5] D. Sun, X. Xu, Y. Qin, S. P. Jiang, Z. Shao, *ChemSusChem* **2020**, *13*, 39–58.
[6] J. T. Feaster, C. Shi, E. R. Cave, T. Hatsukade, D. N. Abram, K. P. Kuhl, C. Hahn, J. K. Nørskov, T. F. Jaramillo, *ACS Catal.* **2017**, *7*, 4822–4827.
[7] C. Kim, H. S. Jeon, T. Eom, M. S. Jee, H. Kim, C. M. Friend, B. K. Min, Y. J. Hwang, *J. Am. Chem. Soc.* **2015**, *137*, 13844–13850.
[8] S. Ma, Y. Lan, G. M. J. Perez, S. Moniri, P. J. A. Kenis, *ChemSusChem* **2014**, *7*, 866–874.
[9] Z. Zhuang, Y. Zhang, L. Hu, J. Wang, Z. Zhang, W. Han, *Adv. Mater. Lett.* **2020**, *11*, 19369–19409.
[10] X. Deng, D. Alfonso, T. D. Nguyen-Phan, D. R. Kauffman, *ACS Catal.* **2022**, *12*, 5921–5929.
[11] S. Zhang, Z. Mo, J. Wang, H. Liu, P. Liu, D. Hu, T. Tan, C. Wang, *Electrochim. Acta* **2021**, *390*, 138831.
[12] J. Huang, M. Mensi, E. Oveisi, V. Mantella, R. Buonsanti, *J. Am. Chem. Soc.* **2019**, *141*, 2490–2499.
[13] G. L. Chai, Z. X. Guo, *Chem. Sci.* **2016**, *7*, 1268–1275.
[14] Z. Sun, T. Ma, H. Tao, Q. Fan, B. Han, *Chem* **2017**, *3*, 560–587.
[15] J. Wu, R. M. Yadav, M. Liu, P. P. Sharma, C. S. Tiwary, L. Ma, X. Zou, X. Zhou, B. I. Yakobson, J. Lou, P. M. Ajayan, *ACS Nano* **2015**, *9*, 5364–5371.
[16] J. Yuan, W. Y. Zhi, L. Liu, M. P. Yang, H. Wang, J. X. Lu, *Electrochim. Acta* **2018**, *282*, 694–701.
[17] B. Kim, F. Hillman, M. Ariyoshi, S. Fujikawa, P. J. A. Kenis, *J. Power Sources* **2016**, *312*, 192–198.
[18] S. C. Perry, S. Mavrikis, M. Wegener, P. Nazarovs, L. Wang, C. Ponce De León, *Faraday Discuss.* **2021**, *230*, 375–387.
[19] M. Li, M. N. Idros, Y. Wu, T. Burdyny, S. Garg, X. S. Zhao, G. Wang, T. E. Rufford, *J. Mater. Chem. A* **2021**, *9*, 19369–19409.
[20] R. Chen, W. Tian, Y. Jia, W. Xu, F. Chen, X. Duan, Q. Xie, C. Hu, W. Liu, Y. Zhao, Y. Kuang, Y. Zhang, X. Sun, *ACS Appl. Energ. Mater.* **2019**, *2*, 3991–3998.
[21] D. Wakerley, S. Lamaison, F. Ozanam, N. Menguy, D. Mercier, P. Marcus, M. Fontecave, V. Mougel, *Nat. Mater.* **2019**, *18*, 1222–1227.
[22] E. A. Hebets, R. F. Chapman, *J. Insect Physiol.* **2000**, *46*, 13–19.
[23] A. T. Le, L. T. Tam, P. D. Tam, P. T. Huy, T. Q. Huy, N. Van Hieu, A. A. Kudrinskiy, Y. A. Krutyakov, *Mater. Sci. Eng. C* **2010**, *30*, 910–916.
[24] W. Quan, X. Wang, C. Song, *Energy Fuels* **2017**, *31*, 9517–9528.
[25] W. Quan, X. Jiang, X. Wang, C. Song, *ACS Sustainable Chem. Eng.* **2020**, *8*, 9998–10008.
[26] J. Chen, X. Liu, S. Xi, T. Zhang, Z. Liu, J. Chen, L. Shen, S. Kawi, L. Wang, *ACS Nano* **2022**, *16*, 13982–13991.
[27] L. Wu, K. E. Kolmeijer, Y. Zhang, H. An, S. Arnouts, S. Bals, T. Altantzis, J. P. Hofmann, M. Costa Figueiredo, E. J. M. Hensen, B. M. Weckhuysen, W. Van Der Stam, *Nanoscale* **2021**, *13*, 4835–4844.
[28] F. Mattarozzi, N. Visser, J. W. De Rijk, P. Ngene, P. De Jongh, *Eur. J. Inorg. Chem.* **2022**, *2022*, 1–8.
[29] D. Tasis, N. Tagmatarchis, A. Bianco, M. Prato, *Chem. Rev.* **2006**, *106*, 1105–1136.
[30] Z. Spitalsky, D. Tasis, K. Papagelis, C. Galiotis, *Prog. Polym. Sci.* **2010**, *35*, 357–401.
[31] T. Bao, Z. Wang, Y. Zhao, Y. Wang, X. Yi, *Materials* **2018**, *11*, 1710.
[32] G. Greczynski, L. Hultman, *Prog. Mater. Sci.* **2020**, *107*, 100591.
[33] G. H Major, N. Fairley, P. M. A. Sherwood, M. R. Lindford, J. Terry, V. Fernandez, K. Artyushkova, *J. Vac. Sci. Technol. A* **2020**, *38*, 031002.
[34] D. J. Morgan, *C – Journal of Carbon Research* **2021**, *7*, 51.

Manuscript received: June 26, 2023
Version of record online: August 21, 2023